Spectral Signal Density of Carotid Plaque Using Dual-Energy Computed Tomography

Exequiel Reynoso, Gastón A. Rodriguez-Granillo, Carlos Capunay, Alejandro Deviggiano, Francisco Meli, Patricia Carrascosa

From the Department of Neuroradiology, Diagnóstico Maipú, Buenos Aires, Argentina (ER, FM); and Department of Cardiovascular Imaging, Diagnóstico Maipú, Buenos Aires, Argentina (GAR-G, CC, AD, PC).

ABSTRACT

BACKGROUND AND PURPOSE: **Plaque characterization using virtual monochromatic imaging derived from dual-energy computed tomography (CT) angiography requires the determination of normal signal density values of each plaque component. We sought to explore the signal density values of carotid plaque components using dual-energy compared to conventional single-energy CT angiography (CTA), and to establish the energy level with the largest differences between plaque components.**

METHODS: **The present prospective study involved consecutive patients referred for carotid artery evaluation by CTA. Two scans (single-energy and dual-energy CTA) were performed in all patients, and a single radiologist analyzed the data. Single-source dual-energy CTA allowed the generation of virtual monochromatic images from 40 to 140 keV.**

RESULTS: **A total of 35 internal carotid artery lesions were examined in 20 symptomatic patients. The mean age was 72.3 ± 6.7 years, and 9 (45%) patients were male. Internal carotid artery geometrical variables including lumen area ($P = .96$), vessel area ($P = .97$), and percent area stenosis ($P = .99$) did not differ between groups (single-energy CTA, and dual-energy CTA at 40, 70, 100, and 140 keV). Differences between signal densities of different tissues were largest at 40 keV (calcium/lumen, $P < .0001$; fat/noncalcified, $P < .0001$).**

CONCLUSIONS: **In the present pilot investigation, virtual monochromatic imaging at low-energy levels derived from dual-energy CTA allowed the largest differences in attenuation levels between tissues, without affecting vessel or plaque geometry.**

Keywords: Carotid plaque imaging, computed tomography, dual energy, atherosclerosis.

Acceptance: Received December 20, 2016. Accepted for publication March 7, 2017.

Correspondence: Address correspondence to Gastón A. Rodriguez-Granillo, MD, PhD, FACC, Department of Cardiovascular Imaging, Diagnóstico Maipú, Av Maipú 1668, Vicente López (B1602ABQ), Buenos Aires, Argentina. E-mail: grodriguezgranillo@gmail.com

Acknowledgment and disclosure sections: We declare that Dr. Patricia Carrascosa is Consultant of GE Healthcare. None of the other authors have conflicts of interest to declare.

J Neuroimaging 2017;00:1-6.
DOI: 10.1111/jon.12440

Introduction

The Asymptomatic Carotid Atherosclerosis Study (ACAS) and the Asymptomatic Carotid Surgery Trial (ACST) have originally established that stenosis severity is not an independent predictor of ipsilateral late stroke.[1,2] In the European Carotid Surgery Trial, 44% of patients with symptomatic carotid stenosis showed only mild angiographic stenosis. Furthermore, the North American Symptomatic Carotid Endarterectomy Trial reported a similar 5-year risk of stroke between patients with 50–69% stenosis and patients with 0–49% stenosis.[3,4] These observations suggested that aside from stenosis severity, plaque composition might be considered an important determinant of plaque instability.[5–7]

More recently, a number of studies showed that some high-risk plaque characteristics such as thin fibrous cap, large lipid core, and intraplaque hemorrhage can be identified or indirectly inferred by means of ultrasound, magnetic resonance imaging (MRI), and conventional computed tomography angiography (CTA).[8–10]

Dual-energy imaging has emerged as a technology with the ability to reduce contrast volume requirements, attenuate blooming, and beam hardening artifacts, and potentially improve tissue characterization. The initial studies using CT dual-energy angiography (CTA-DE) have shown promising findings in this regard, demonstrating a high sensitivity for the detection of mixed and low-density fatty plaques.[11] More recently, effective z-maps derived from dual energy have shown potential to discriminate between vulnerable and stable plaques.[12] An alternative approach for tissue characterization using dual energy comprises virtual monochromatic imaging (VMI). For this purpose, it is pivotal to establish normal signal density (SD) values of each plaque component at each monoenergetic level. Therefore, the aim of this study was to explore the SD values of carotid plaque components using dual-energy compared to conventional single-energy CT angiography (CTA), and to establish the energy level with the largest differences between plaque components.

Materials and Methods

Patient Population

The present single-center, investigator-driven, prospective study involved consecutive patients referred for carotid artery evaluation by CTA in our institution. Two scans were performed in all patients: single-energy CTA (CTA-SE), and dual-energy CTA (CTA-DE). All patients were more than 18 years

old, without a history of contrast related allergy, renal failure, or hemodynamic instability. Additional exclusion criteria comprised a body mass index larger than 32 kg/m^2, a history of bilateral carotid percutaneous revascularization, or carotid bypass graft surgery.

CTA-SE and CTA-DE Acquisitions

Patients were scanned using a 64-detector row dual-energy CT scanner (Discovery HD 750, GE Healthcare, Milwaukee, WI, USA) equipped with gemstone spectral imaging. CTA-DE was acquired through rapid switching (.3 to .5 milliseconds) between high and low tube potentials (80–140 kV) from a single source, allowing the reconstruction of low- and high-energy projections and generation of monochromatic image reconstructions ranging from 40 to 140 keV. Sequentially, two acquisitions were performed in each patient from the aortic arch to the base of the skull in caudocranial direction: CTA-SE and CTA-DE. Using an antecubital venous access, both acquisitions were performed after injection of a 50 to 60 mL bolus of iodinated contrast (iobitridol, Xenetix^{TM}, 350 mg I/mL, Guerbet, France) at flow rate of 4.5 mL/seconds, followed by a 40 mL saline chaser using the same flow rate. Scan delay was determined using a test bolus method. CTA-SE was performed using the following acquisition parameters: slice thickness, .625 mm; rotation speed, .5 seconds; tube voltage, 100 kVp; tube current, 300 mA; pitch .984:1; and matrix, 512 × 512. CTA-DE acquisition was performed using the following parameters: slice thickness, .625 mm; rotation speed, .5 seconds; tube voltage, fast-kV switching between 80 and 140 kVp; tube current, 630 mA; pitch .984:1; and matrix, 512 × 512. CTA-DE acquisitions allowed the generation of VMI from 40 to 140 keV.

Image Analysis

Image analysis was performed offline by an experienced radiologist in a dedicated workstation using commercially available software (AW 4.6, GE Healthcare). The same observer analyzed the CTA-SE dataset and, 30 days later, the CTA-DE dataset at four independent monoenergetic (40, 70, 100, and 140 keV) reconstructions. Iterative reconstruction was applied at 50% adaptive statistical iterative reconstruction (ASIR) for CTA-SE datasets and for CTA-DE datasets (70, 100, and 140 keV). With the current software, 60 keV is the lowest monoenergetic level available for reconstructions with ASIR. Window level and width for this purpose were at the observer's discretion. All analyses were performed at the site of maximum stenosis and at a distal reference segment with minimal or no evidence of atherosclerosis. Carotid plaque analysis was performed for each patient initially using multiplanar reconstructions and orthogonal views at the cross-sectional area (CSA) of the internal carotid artery with the highest degree of stenosis. Care was taken to identify the carotid bifurcation at the same slice and projection across all datasets, using anatomical landmarks as reference. Manual planimetry of the lumen CSA and vessel CSA was performed both at the site of maximum stenosis and at the distal reference segment. The plaque CSA was derived from these measurements ($vessel_{csa}$ – $lumen_{csa}$). The degree of carotid artery stenosis was defined using the percent area stenosis as suggested by the European Carotid Surgery Trial ($vessel_{CSA} - lumen_{CSA}/vessel_{area} \times 100$).[13] The SD of each tissue (perivascular fat, lumen, and two different carotid plaque tissue types: calcium and noncalcified plaque with the lowest SD) was measured (in Hounsfield units [HUs]). Given the small size and heterogeneity of carotid plaque tissues and thus the inability to standardize regions of interest for every patient, we decided to use a pixel lens (Fig 1). This was performed with particular care to target the core of the tissue component (after sampling three regions and selecting the mid measurement) and to avoid regions affected by beam hardening artifacts.

The effective radiation dose with CTA-SE and CTA-DE was also estimated and obtained using the correction factor as suggested by international standards.[14] The institutional review board approved the study protocol, which complied with the Declaration of Helsinki, and written informed consent was obtained from all patients.

Statistical Analysis

Discrete variables are presented as counts and percentages. Continuous variables are presented as means ± standard deviation. Comparisons among groups were performed using paired samples *t*-tests, and one way analysis of variance (post-hoc comparisons with Bonferroni tests). Nonparametric correlations between variables were performed using Spearman correlation coefficients. In order to test the reproducibility of our findings, the same observed performed 4 months after the original analysis a densitometric analysis of the ICA at CTA-SE and CTA-DE at all energy levels for lumen SD, calcium SD, noncalcified plaque SD, and perivascular fat SD. The intraobserver variability was assessed using intraclass correlation coefficients (using a two-way random effect model, absolute agreement, and average measurement) with 95% confidence intervals. All statistical analyses were performed using SPSS software, version 22.0 (Chicago, Illinois, USA). A two-sided *P* value of less than .05 indicated statistical significance.

Results

A total of 35 internal carotid artery bifurcation lesions were examined in 20 symptomatic patients and prospectively included in the study protocol. One vessel was excluded from the analysis due to previous carotid stenting. The effective radiation dose, although very low with both techniques, was significantly lower using CTA-SE compared to CTA-DE (1.45 ± .1 mSv vs. 1.75 ± .2 mSv, $P < .0001$). Based on CTA-SE, 21 (54%) internal carotid arteries had mild (<50%) stenosis, 5 (13%) had moderate (50–69%) stenosis, 9 (23%) had severe (70–99%) stenosis, and 4 vessels were totally occluded. The later were excluded from the analysis as prespecified in the study protocol. On a per-patient basis, the maximum stenosis severity was the following: 6 (30%) mild stenosis; 2 (10%) moderate stenosis; 8 (40%) severe stenosis; and 4 had total occlusion.

The mean age was 72.3 ± 6.7 years, and 9 (45%) patients were male. Seventeen (85%) patients had hypertension, 14 (70%) hypercholesterolemia, 2 (10%) diabetes, and 1 (5%) patient was a current smoker. The mean body mass index was 27.4 ± 2.9 kg/m^2. Eight (40%) patients were included due to a previous history of ischemic stroke, whereas 12 (60%) patients were included due to transient ischemic attack.

Carotid Plaque Analysis

The mean internal carotid artery percent area obstruction was 62 ± 19% at CTA-SE assessment, with no significant differences compared to CTA-DE. The other vessel geometrical variables

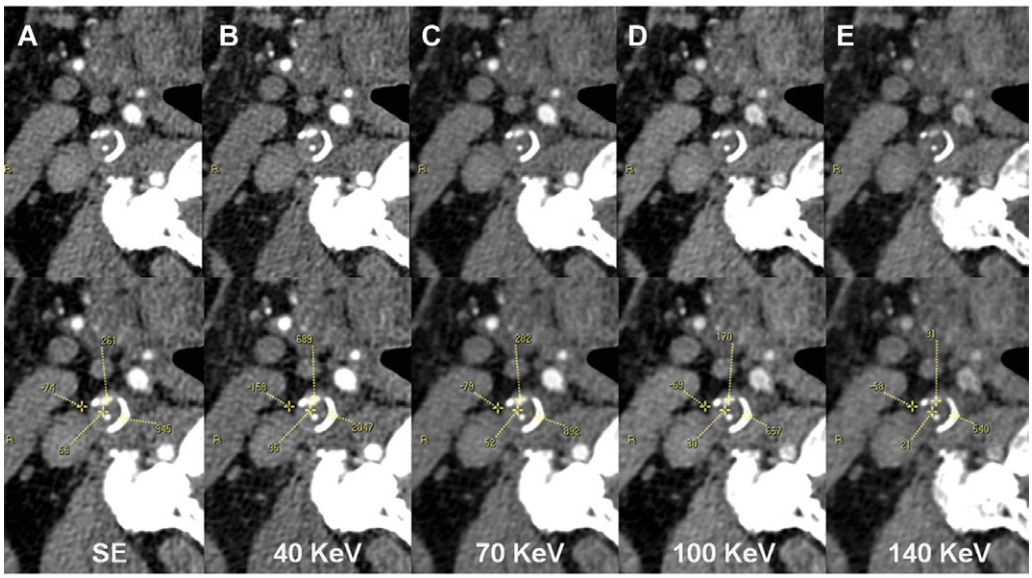

Fig 1. Sixty-three-year old male with right internal carotid plaque. Orthogonal views of the internal carotid artery at the bifurcation level using single-energy CT angiography (A) and dual-energy CT at of 40, 70, 100, and 140 keV (B–E). Densitometric analyses (in Hounsfield units) of intraluminal (12 o'clock), perivascular fat, calcium, and noncalcified tissues are depicted.

Table 1. Geometrical Analysis. Computed Tomography Angiography Using Single-Energy (CTA-SE) and Dual-Energy (CTA-DE) Acquisitions

	Lumen (mm^2)	Vessel (mm^2)	Calcium (mm^2)	Area Stenosis (%)
CTA-SE	22 ± 12	60 ± 19	12 ± 17	62 ± 19
CTA-DE				
40 keV	22 ± 12	60 ± 17	13 ± 24	62 ± 20
70 keV	22 ± 12	62 ± 18	10 ± 14	62 ± 21
100 keV	22 ± 12	61 ± 17	9 ± 12	63 ± 21
140 keV	21 ± 11	60 ± 19	8 ± 12†	64 ± 20
P^*	.96	.97	.60	.99

*P (ANOVA across CTA-DE); †$P = .07$ versus CTA-SE.

(lumen and vessel CSA) did not differ between groups neither at the site of maximum stenosis, nor at the distal reference (Table 1, Figs 1 and 2).

Among the CTA-DE group, lumen and calcium SD values were significantly higher at the lowest energy level (40 keV), rapidly decreasing at increasing energy levels (Table 2). Perivascular fat and noncalcified plaque SD levels gradually increased and declined, respectively, at increasing energy levels (Table 2).

SD levels of the internal carotid artery lumen, calcium, noncalcified plaque, and perivascular fat were similar between CTA-SE and CTA-DE at 70 keV (lumen 341 ± 210 HU vs. 327 ± 162 HU; calcium 834 ± 296 HU vs. 774 ± 347 HU; noncalcified plaque 81 ± 51 HU vs. 80 ± 62 HU; and perivascular fat −91 ± 39 HU vs. −96 ± 43 HU; with nonsignificant differences across all paired comparisons).

The differences between signal densities of different tissues were larger using the lowest energy level (40 keV) (Fig 3).

There was an excellent intraobserver agreement for all tissues using CTA-SE (fat: k .98 [95% CI .97–.99], $P < .0001$; lumen: k .99 [95% CI .98–1.0], $P < .0001$; calcium: k .99 [95% CI .97–.99], $P < .0001$; and noncalcified plaque: k .99 [95% CI .97–.99], $P < .0001$). The intraobserver agreement using CTA-DE across all energy levels was as follows (fat: k .90 [95% CI .86–.93], $P < .0001$; lumen: k .99 [95% CI .99–1.0], $P < .0001$; calcium: k .99 [95% CI .99–1.0], $P < .0001$; and noncalcified plaque: k .93 [95% CI .91–.95], $P < .0001$).

Relationship between Luminal Attenuation Levels and Density of Plaque Components

We identified a significant correlation between the luminal SD levels and the attenuation level of noncalcified plaques only at 40 keV reconstructions ($r = .43$, $P = .01$), whereas we did not find significant relationships between luminal and noncalcified plaque SD levels among CTA-SE ($r = .14$, $P = .42$), or CTA-DE at 70 keV ($r = .14$, $P = .43$), 100 keV ($r = .33$, $P = .054$), or 140 keV ($r = .13$, $P = .47$).

On the contrary, no significant correlations were identified between the lumen SD levels and the attenuation levels of calcified plaques among neither CTA-SE ($r = .19$, $p = .27$), nor CTA-DE at 40 keV ($r = .26$, $p = .14$), 70 keV ($r = .19$, $p = .28$), 100 keV ($r = .17$, $P = .33$), or 140 keV ($r = -.06$, $P = .74$). Similarly, no significant relationships were found between lumen SD levels and the SD levels of perivascular fat among neither CTA-SE ($r = -.06$, $P = .74$), nor CTA-DE at 40 keV ($r = .02$, $P = .92$), 70 keV ($r = -.21$, $P = .24$), 100 keV ($r = -.12$, $P = .49$), or 140 keV ($r = .18$, $P = .31$).

Discussion

The main finding of the present study was that VMI at low-energy levels derived from dual-energy CTA allowed the largest differences in attenuation levels between carotid plaque tissues, without affecting vessel or plaque geometry.

Recent data emerging from robust clinical studies suggest that patients with extensive but nonobstructive coronary atherosclerosis have similar or even worse clinical outcome than patients with obstructive but nonextensive disease.[15,16] These findings, along with the aforementioned results from the ACAS

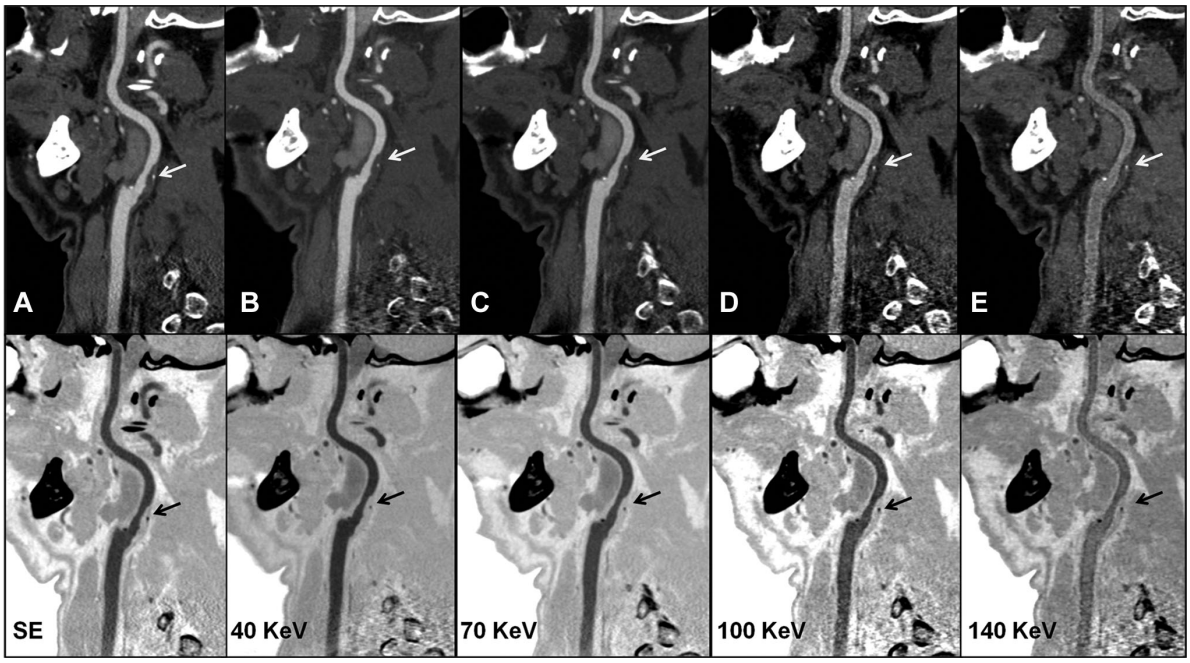

Fig 2. Seventy-five-year old male with left internal carotid plaque. Curved multiplanar reconstructions of the common and internal carotid artery using single-energy CT angiography (A) and dual-energy CT at of 40, 70, 100, and 140 keV (B–E). No significant variation in plaque geometry is observed (arrow).

Table 2. Signal Density Analyses of Carotid Plaques and Surroundings by Computed Tomography Angiography Using Single-Energy (CTA-SE) and Dual-Energy (CTA-DE) Acquisitions

	Fat (HU)	Calcium (HU)	NCP (HU)	Lumen (HU)
CTA-SE	−91 ± 38	834 ± 296	81 ± 51	341 ± 210
CTA-DE				
40 keV	−180 ± 100*	1,698 ± 654*	166 ± 112*	846 ± 244*
70 keV	−96 ± 43	774 ± 347	80 ± 62	327 ± 162
100 keV	−72 ± 17*	548 ± 228*	52 ± 34*	163 ± 37*
140 keV	−63 ± 16*	450 ± 219*	54 ± 73*	104 ± 34*
P (ANOVA across DECT)	<.0001	<.0001	<.0001	<.0001

*denotes significant paired differences versus single-energy CT. NCP refers to noncalcified plaque. CTA-SE = computed tomography angiography single energy; CTA-DE = computed tomography angiography dual energy; SE = single energy; DE = dual energy; HU = Hounsfield units.

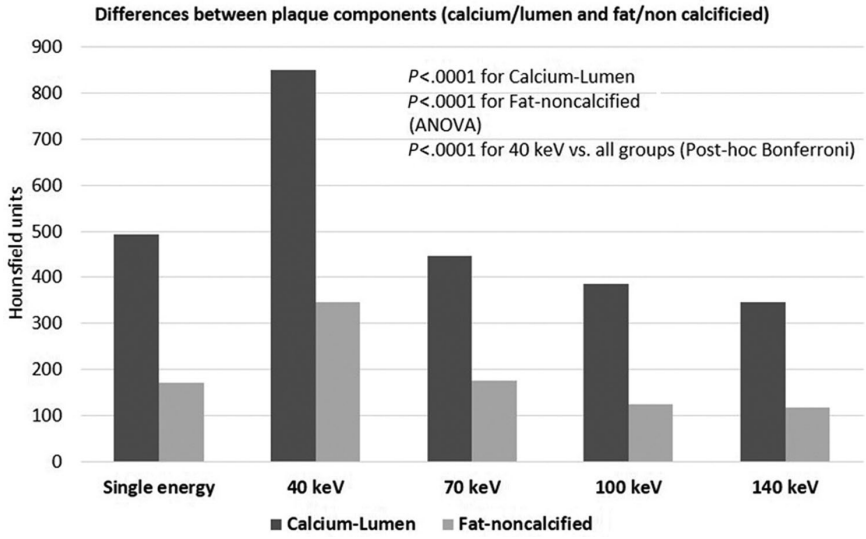

Fig 3. Signal density (in Hounsfield units) differences of plaque components (calcium/lumen and fat/noncalcified plaque) using single-energy CT angiography and dual-energy CT angiography at increasing energy levels (40, 70, 100, and 140 keV).

and ACST studies, underscore the need for significant improvement in risk prediction strategies based on accurate noninvasive plaque characterization.

Advanced carotid plaque imaging by means of MRI has emerged as a tool with the ability to assess a number of high-risk features such as lipid content, intraplaque hemorrhage, and even to infer fibrous cap thickness.[17,18] Although MRI is the gold standard for carotid plaque imaging, this technique has a number of limitations including high cost and long scanning times, along with recent safety concerns (albeit probably overemphasized) including reports of DNA double-strand breaks and gadolinium-associated nephrogenic systemic fibrosis and deposition in the skin and brain.[19–21] Carotid plaque imaging by means of CTA allows fast high-resolution imaging and can accurately detect ulceration, calcification, and low attenuation plaques suggestive underlying high-risk features, although it cannot reliably discriminate between lipid-rich plaques, fibrotic plaques, and intraplaque hemorrhage.[22] Furthermore, the role of CTA might be particularly useful among patients with claustrophobia and/or with implantable cardiac devices.

SD Levels with Single- and Dual-Energy Imaging

Dual-energy imaging has emerged as a novel approach with the potential to attenuate several technical limitations of conventional single-energy CT, and a number of studies have showed the ability of VMI to improve grading of diffusely calcified carotid artery stenosis, and even tissue characterization.[23] Dual-energy imaging has the potential to analyze the information using two different approaches: monochromatic evaluation and material decomposition. Shinohara et al. recently reported an inverse relationship between effective Z values (based on effective atomic numbers) derived from CTA-DE and the extent of fibrofatty tissue assessed by spectral radiofrequency data analysis within carotid plaques. The authors concluded that CTA-DE can detect vulnerable plaque material. Though hypothesis generating, it is worth mentioning that the so-called vulnerable plaque material is typically the necrotic core, not the fibrofatty tissue. Indeed, recent studies have shown a significant reduction in the necrotic core and plaque volumes with moderate to high statin doses, whereas the fibrofatty volume increased significantly.

Standardization of SD values of carotid plaque components is pivotal in order to perform plaque characterization with VMI by means of CTA-DE. Previous studies have reported mean SD values of fatty plaques (35 ± 25 HU), mixed plaques (51 ± 19 HU), and calcified plaques (290 ± 53 HU) using CTA-SE.[11]

Our study is the first that prospectively explored the SD of carotid plaque components with both CTA-SE and CTA-DE (at several monoenergetic levels).

Our findings can be summarized as follows. First, internal carotid artery geometrical variables, such as lumen area, vessel area, and percent area stenosis, did not differ between CTA-SE and CTA-DE (at any energy level). Nevertheless, in line with previous findings from a very small ex-vivo study suggesting that the most accurate estimates of calcification size was 80–100 keV, calcified areas gradually declined at increasing energy levels.[24] Furthermore, SD of calcium, noncalcified plaque, and lumen (iodine) significantly declined at increasing energy levels; whereas the behavior of fat SD, devoid from iodine, was the opposite.

It is noteworthy that the largest differences between tissue components were observed at the lowest energy level (40 keV). In particular, the largest SD differences between tissues that commonly have similar SD such as calcium/lumen and noncalcified plaque/fat were observed at 40 keV. In addition, we identified an intriguing albeit weak correlation between the luminal SD levels and the attenuation level of noncalcified plaques only at 40 keV reconstructions, whereas no significant correlations were identified between the lumen SD levels and the attenuation levels of calcified plaques or perivascular fat.

These findings appear to be in agreement with recent data showing that low-energy levels, which typically depict the highest SD and the highest image noise, have the highest diagnostic performance to detect myocardial perfusion defects and delayed enhancement (unpublished data).

It is expected that with the upcoming iterative reconstruction algorithm available for all energy levels (with current version only for $\geq$60 keV), contrast to noise ratio of the lowest energy levels will experience major improvements. Overall, our findings warrant further larger investigations exploring histopathological correlates of precontrast, contrast, and delayed enhancement imaging of (predominantly noncalcified) carotid plaques. Furthermore, future studies should explore whether CTA-DE might become an alternative for carotid plaque MRI in selected populations.

A number of limitations of our study should be recognized. The relatively small sample size might lead to selection bias. Furthermore, histopathological data were not available as a reference standard for carotid plaque characterization. We recognize that the definition of tissue types based on manual determination at specific sites may lead to sampling bias. However, manually delineating standardized regions of interest may lead to a systematic bias, as small calcifications or fat depositions in mixed areas have an impact on pixel density. Furthermore, automated border detection algorithms are not well validated. Finally, we did not perform delayed enhancement acquisitions, which have been related to intraplaque hemorrhage in MRI.

Conclusions

In the present pilot investigation, VMI at low-energy levels derived from CTA-DE allowed the largest differences in attenuation levels, without affecting vessel or plaque geometry.

References

1. Endarterectomy for asymptomatic carotid artery stenosis. Executive Committee for the Asymptomatic Carotid Atherosclerosis Study. JAMA 1995;273:1421-8.
2. Halliday A, Mansfield A, Marro J, et al. Prevention of disabling and fatal strokes by successful carotid endarterectomy in patients without recent neurological symptoms: randomised controlled trial. Lancet 2004;363:1491-502.
3. Rothwell PM, Gutnikov SA, Warlow CP, European Carotid Surgery Trialist's Collaboration. Reanalysis of the final results of the European Carotid Surgery Trial. Stroke 2003;34:514-23.
4. Barnett HJ, Taylor DW, Eliasziw M, et al. Benefit of carotid endarterectomy in patients with symptomatic moderate or severe stenosis. North American Symptomatic Carotid Endarterectomy Trial Collaborators. N Engl J Med 1998;339:1415-25.
5. Streifler JY, Eliasziw M, Fox AJ, et al. Angiographic detection of carotid plaque ulceration. Comparison with surgical observations in a multicenter study. North American Symptomatic Carotid Endarterectomy Trial. Stroke 1994;25:1130-2.

6. Lovett JK, Gallagher PJ, Hands LJ, et al. Histological correlates of carotid plaque surface morphology on lumen contrast imaging. Circulation 2004;110:2190-7.
7. Naghavi M, Libby P, Falk E, et al. From vulnerable plaque to vulnerable patient: a call for new definitions and risk assessment strategies: Part II. Circulation 2003;108:1772-8.
8. Standish BA, Spears J, Marotta TR, et al. Vascular wall imaging of vulnerable atherosclerotic carotid plaques: current state of the art and potential future of endovascular optical coherence tomography. AJNR Am J Neuroradiol 2012;33:1642-50.
9. Truijman MT, Kooi ME, van Dijk AC, et al. Plaque At RISK (PARISK): prospective multicenter study to improve diagnosis of high-risk carotid plaques. Int J Stroke 2014;9:747-54.
10. de Rotte AA, Truijman MT, van Dijk AC, et al. Plaque components in symptomatic moderately stenosed carotid arteries related to cerebral infarcts: the plaque at RISK study. Stroke 2015;46:568-71.
11. Das M, Braunschweig T, Muhlenbruch G, et al. Carotid plaque analysis: comparison of dual-source computed tomography (CT) findings and histopathological correlation. Eur J Vasc Endovasc Surg 2009;38:14-9.
12. Shinohara Y, Sakamoto M, Kuya K, et al. Assessment of carotid plaque composition using fast-kV switching dual-energy CT with gemstone detector: comparison with extracorporeal and virtual histology-intravascular ultrasound. Neuroradiology 2015;57:889-95.
13. MRC European Carotid Surgery Trial: interim results for symptomatic patients with severe (70–99%) or with mild (0–29%) carotid stenosis. European Carotid Surgery Trialists' Collaborative Group. Lancet 1991;337:1235-43.
14. European guidelines on quality criteria for computed tomography. Available at: http://www.drs.dk/guidelines/ct/quality/htmlindex.htm. Accessed August 2016.
15. Maddox TM, Stanislawski MA, Grunwald GK, et al. Nonobstructive coronary artery disease and risk of myocardial infarction. JAMA 2014;312:1754-63.
16. Bittencourt MS, Hulten E, Ghoshhajra B, et al. Prognostic value of nonobstructive and obstructive coronary artery disease detected by coronary computed tomography angiography to identify cardiovascular events. Circ Cardiovasc Imaging 2014;7:282-91.
17. Millon A, Mathevet JL, Boussel L, et al. High-resolution magnetic resonance imaging of carotid atherosclerosis identifies vulnerable carotid plaques. J Vasc Surg 2013;57:1046-51.e2.
18. Sun J, Zhao XQ, Balu N, et al. Carotid magnetic resonance imaging for monitoring atherosclerotic plaque progression: a multicenter reproducibility study. Int J Cardiovasc Imaging 2015;31:95-103.
19. Lancellotti P, Nchimi A, Delierneux C, et al. Biological effects of cardiac magnetic resonance on human blood cells. Circ Cardiovasc Imaging 2015;8:e003697. https://doi.org/10.1161/CIRCIMAGING.115.003697
20. Stojanov D, Aracki-Trenkic A, Benedeto-Stojanov D. Gadolinium deposition within the dentate nucleus and globus pallidus after repeated administrations of gadolinium-based contrast agents-current status. Neuroradiology 2016;58:433-41.
21. Roberts DR, Lindhorst SM, Welsh CT, et al. High levels of gadolinium deposition in the skin of a patient with normal renal function. Invest Radiol 2016;51:280-9.
22. Brinjikji W, Huston J, 3rd, Rabinstein AA, et al. Contemporary carotid imaging: from degree of stenosis to plaque vulnerability. J Neurosurg 2016;124:27-42.
23. Korn A, Bender B, Brodoefel H, et al. Grading of carotid artery stenosis in the presence of extensive calcifications: dual-energy CT angiography in comparison with contrast-enhanced MR angiography. Clin Neuroradiol 2015;25:33-40.
24. Mannelli L, MacDonald L, Mancini M, et al. Dual energy computed tomography quantification of carotid plaques calcification: comparison between monochromatic and polychromatic energies with pathology correlation. Eur Radiol 2015;25:1238-46.